Radiation-induced defects in quartz. II. Single-crystal W-band EPR study of a natural citrine quartz

Article *in* Physics and Chemistry of Minerals · April 2008

DOI: 10.1007/s00269-008-0233-7

3 authors, including:

Rudolf I. Mashkovtsev
Sobolev Institute of Geology and Mineralogy
58 PUBLICATIONS **395** CITATIONS

Phys Chem Minerals (2008) 35:387–397
DOI 10.1007/s00269-008-0233-7

ORIGINAL PAPER

Radiation-induced defects in quartz. II. Single-crystal W-band EPR study of a natural citrine quartz

Yuanming Pan · Mark J. Nilges · Rudolf I. Mashkovtsev

Received: 11 November 2007 / Accepted: 17 March 2008 / Published online: 2 April 2008

Abstract Single-crystal electron paramagnetic resonance (EPR) spectra of a natural citrine quartz without any artificial irradiation, measured at W-band frequencies (~94 GHz) and temperatures of 77, 110 and 298 K, allow better characterization of three previously-reported Centers (#6, #7 and B) and discovery of three new defects (B′, C′ and G′). The W-band EPR spectra reveal that Centers #6 and #7 do not reside on twofold symmetry axes, contrary to results from a previous X-band EPR study. The W-band spectra also show that the previously reported Center B is a mixture of two defects (B and B′) with similar *g* matrices but different-sized ^{27}Al hyperfine structures. Center C′ has similar principal *g* values to the previously reported Center C but is distinct from the latter by a larger ^{27}Al hyperfine structure with splittings from 0.10 to 0.22 mT. Also, Center G′ has a similar *g* matrix to the previously reported Center G but a different ^{27}Al hyperfine structure with splittings from 0.41 to 0.53 mT. These spin-Hamiltonian parameters, together with observed thermal properties and microwave-power dependence, suggest that Centers #6 and #7 probably represent O_2^{3-} type defects. Centers B and B′ are probably superoxide radicals (O_2^-) with the unpaired spin localized on the same pair of oxygen atoms around a missing Si atom but linked to a substitutional Al^{3+} ion each at different neighboring tetrahedral sites. Similarly, Centers G and G′ are most likely superoxide radicals with the unpaired spin localized on another pair of oxygen atoms around a missing Si atom and linked to a substitutional Al^{3+} ion each at different neighboring tetrahedral sites. Center C′ is probably an ozonide radical associated with a missing Si atom and linked to a substitutional Al^{3+} ion at the neighboring tetrahedral site. This study exemplifies the value of high-frequency EPR for discrimination of similar defect centers and determination of small local structural distortions that are often difficult to resolve in conventional X- and Q-band EPR studies.

Keywords Natural citrine quartz · Radiation-induced defects · Single-crystal W-band EPR · Symmetry · ^{27}Al hyperfine structures · O_2^- · O_2^{3-} and O_3^- centers

Y. Pan (✉) · R. I. Mashkovtsev
Department of Geological Sciences,
University of Saskatchewan, Saskatoon,
SK, Canada S7N 5E2
e-mail: yuanming.pan@usask.ca

M. J. Nilges
Illinois EPR Research Center,
University of Illinois at Urbana-Champaign,
Urbana, IL 61801, USA

R. I. Mashkovtsev
Institute of Geology and Mineralogy,
Siberian Branch of Russian Academy of Sciences,
630090 Novosibirsk, Russia

Introduction

Citrine quartz includes a number of colored varieties from yellow to orange and orange brown (Schmetzer 1989; Rossman 1994 and references therein). Substitutional Fe^{3+} ions or submicroscopic Fe_2O_3 particles have been proposed to be responsible for the brownish varieties (e.g., heat-treated amethyst; Schmetzer 1989; Rossman 1994). Several previous studies (Samoilovich et al. 1969, 1976; Maschmeyer et al. 1980; Maschmeyer and Lehmann 1983) noted that the yellow varieties are distinct from their iron-containing counterparts and contain a number of hole-like paramagnetic centers, in addition to the more common

$[AlO_4]^0$ and $[AlO_4]/M^+$ centers (where $M = Na^+$, Li^+ and H^+; Weil 1984; Walsby et al. 2003 and references therein). Most of these hole-like centers have since been found to occur in quartz from the uranium-rich Athabasca basin (Botis et al. 2005, 2008), and are also known to occur in artificially irradiated samples (Mashkovtsev et al. 1978; Azzoni et al. 1994; Nilges et al. 2008), apparently representing radiation-induced defects.

In part I of this series (Nilges et al. 2008), the W-band EPR spectra of an electron-irradiated, natural quartz showed that two radiation-induced defects (i.e., Center #1 similar to Center F in citrine and an ozonide radical), which were reported by previous X- and Q-band EPR studies to reside on twofold symmetry axes in the quartz structure (Mashkovtsev et al. 1978; Maschmeyer and Lehmann 1983; Botis et al. 2008), in fact deviate from twofold axes by $\sim 2°$ and $\sim 10°$, respectively. Similarly, the W-band EPR spectra showed that the direction of the *g*-intermediate axis of Center G, which was also first discovered in citrine and suggested by a Q-band EPR study to coincide with the direction perpendicular to both threefold and twofold symmetry axes (Maschmeyer and Lehmann 1983), is actually $\sim 5°$ away from that direction. In addition, the W-band EPR spectra of the electron-irradiated quartz disclosed Center #6 of Mashkovtsev et al. 1978) and showed it to possess six magnetically nonequivalent sites, although two of them are generally invisible owing to significant difference in site population in that sample (Nilges et al. 2008). Center #6 is similar in its reported principal *g* values and observed magnitudes of ^{29}Si hyperfine splittings to the well-established peroxy radical (i.e., $\equiv Si-O-O\bullet$, where $\equiv$ represents three Si−O bonds and • denotes the unpaired electron) in amorphous silica (Friebele et al. 1979; Griscom and Friebele 1981), and peroxy radicals in quartz have long been proposed to be useful in paleodosimetry and EPR dating (Garrison et al. 1981; Ikeya 1993). The W-band EPR spectra of this electron-irradiated quartz suggested that the spin-Hamiltonian parameters of Center #6 reported by Mashkovtsev et al. (1978) may contain significant error. Unfortunately, the W-band EPR spectra of the electron-irradiated quartz did not allow a quantitative analysis of Center #6, because of not only significant difference in site population but also considerable line-broadening even at 77 K (Nilges et al. 2008).

Accordingly, we reinvestigated the natural citrine quartz of Mashkovtsev et al. (1978), which has not been subject to any artificial irradiation and was used in the original description of Center #6 (and #7), by use of single-crystal EPR spectroscopy at W-band frequencies. The W-band spectra reported herein allow a better characterization of Centers #6 and #7 and disclose four other centers (B, B′, C′ and G′), of which Centers B′, C′ and G′ are new defects in quartz. In particular, both Centers #6 and #7 are confirmed to possess six magnetically non-equivalent sites and, therefore, do not reside on twofold axes. Also, the W-band EPR spectra reveal that Center B reported by Maschmeyer et al. (1980) is a mixture of two similar centers, which can not be resolved at X- or Q-band frequencies. The new spin-Hamiltonian parameters of these centers, together with thermal properties and saturation behavior, provide new insights into their structural models.

Sample, experimental procedures and data analysis

The natural citrine quartz from Ural, Russia (Mashkovtsev et al. 1978), was a yellow, rounded grain of ~ 3 mm in diameter. This grain was sawed into two halves, and one of them was annealed in air at 400°C for 24 h. Both halves were first measured at X-band frequencies and then broken into smaller pieces for field-swept W-band EPR measurements on a home-built spectrometer (Nilges et al. 1999) at the Illinois EPR Research Center (IERC), University of Illinois at Urbana-Champaign. Procedures and conditions of W-band experiments are similar to those described in part I, except that measurements at 298, 110 and 77 K and various microwave powers were made with the Zeeman magnetic field **B** in two approximately orthogonal planes, one of which was chosen arbitrarily owing to the lack of any morphological features for crystal alignment. We used a specially designed TE103 cavity similar to that described in Nilges et al. (1999), except with the addition of a geared rotating mount for the silica tube that supports the crystal. The gearing is 10° for every turn of the control rod. B-field calibration was carried out by use of a Metrolab NMR teslameter PT2025 (Nilges et al. 1999).

All data analyses including angle corrections, optimization of spin-Hamiltoninan parameters and spectral simulations were made by use of the EPR-NMR software package of Mombourquette et al. (1996). Angle corrections to determine the crystal orientations were first made on the basis of the well-characterized E_1' center (298 and 110 K; Jani et al. 1983) and the $[AlO_4]^0$ center (77 K; Walsby et al. 2003). Subsequently, angle corrections were made again during iterative fitting for each of six centers investigated in this study (Table 1). Confidence in this method of angle corrections is demonstrated by the fact that results from different centers agree within 0.08° at 77 K and 0.1° at both 110 and 298 K, within experimental uncertainties in crystal rotation of approximately 0.2°.

The spin-Hamiltonian used in interpreting the EPR spectra of this study takes the form:

$$H_S = \beta_e \mathbf{S} \cdot \mathbf{g} \cdot \mathbf{B} + \mathbf{S} \cdot \mathbf{A} \cdot \mathbf{I} - \beta_n \mathbf{I} \cdot \mathbf{g_n} \cdot \mathbf{B} + \mathbf{I} \cdot \mathbf{P} \cdot \mathbf{I},$$

where β_e, β_n, **S** and **I** are the electron magneton, nuclear magneton, electronic operator and nuclear operator, respectively. The parameters to be optimized are matrices

g, **A** and **P**. Of the six centers analyzed in this study (Table 1), the spin-Hamiltonian parameters of Centers #6, B and G′ have been determined from EPR spectra measured at two temperatures each, whereas those of Centers #7, B′ and C′ have been determined from spectra collected at only one temperature each. Table 1 also gives the numbers of line-position data points used for each center. A low weight factor of 0.1 was assigned to lines that are difficult to measure owing to peak overlapping. Optimizations of spin-Hamiltonian parameters were generally stopped when all elements in the *g* matrices reach the fifth decimal point in significant number, corresponding to the root-mean-sum of squares of the weighted difference (RMSD) between the calculated and observed line-position data to ≤0.16 mT (Table 1), except for 0.213 mT for Center B′ at 298 K owing to its low intensity and peak overlapping (see below). Following previous studies (e.g., Weil 1984; Walsby et al. 2003), we adopted a negative sign for the isotropic part of **A** for ^{27}Al hyperfine structures (Table 1). Nuclear quadrupole matrices **P**, which were also included in the analysis of ^{27}Al hyperfine structures of Centers B, B′ and C′, are all small and cannot be tightly constrained by W-band data, hence not listed in Table 1. Table 2 also includes the principal *g* values of the E_1' center from the W-band spectra of this study, for comparison with those reported by Jani et al. (1983).

Results

The citrine crystal became colorless after annealing in air at 400°C for 24 h. X- and W-band EPR measurements of the annealed crystal at various microwave powers and temperatures did not detect any paramagnetic center, except for a weak E_1' signal. Therefore, all descriptions of paramagnetic defects in the citrine quartz below are based on spectra measured on the pieces without annealing.

Single-crystal X-band spectra of the citrine quartz are dominated by the E_1' center (Fig. 1). Other paramagnetic centers, including "Center B" of Maschmeyer et al. (1980), are also disclosed but are invariably low in signal-to-noise ratios (Fig. 1). The X-band EPR spectra of this citrine quartz are broadly similar to those of drusy quartz from the uranium-rich Athabasca basin (Botis et al. 2008).

Single-crystal W-band spectra measured at 298, 110 and 77 K are all composed of a large number of resonance absorption lines (Fig. 2), hence much richer in structure than their X-band counterparts. On the basis of thermal properties, microwave-power dependence, and the presence or absence of ^{27}Al hyperfine structures, we are able to identify ten defects in this sample: E_1' (Jani et al. 1983), $[AlO_4]^0$ (Walsby et al. 2003), Centers #6 and #7 of Mashkovtsev et al. (1978) (Fig. 2a, b), Centers D and E of Maschmeyer and Lehmann (1983), two defects similar to "Center B" of Maschmeyer et al. (1980) (B and B′; Fig. 2c), and two new centers (C′ and G′; Fig. 2c). However, Centers D and E, along with numerous other peaks with or without ^{27}Al hyperfine structures, are low in intensity and difficult to follow relative to crystal rotation and, therefore, are not discussed further here.

The single-crystal W-band EPR spectra decrease in intensity away from the field region of free electron ($g = 2.0023$; Fig. 2a, b), pointing to *g*-strain effects. However, difference in line intensity among magnetically non-equivalent sites, which is significant in the W-band EPR spectra of the electron-irradiated quartz (Nilges et al. 2008), is less severe here. For example, the W-band spectra of the $[AlO_4]^0$ center have all six sites well resolved (Fig. 2a), in contrast to four visible sites in the electron-irradiated crystal (Nilges et al. 2008) and only two visible sites in an X-irradiated synthetic quartz (Mackey et al. 1970).

Center #6

Center #6 is well-resolved at 77 K (Fig. 2a) and 110 K (Fig. 2b), but is not detectable at 298 K (Fig. 2c; see also Mashkovtsev et al. 1978). At 77 and 110 K, Center #6 is best resolved at microwave powers ≥6.3 mW, when other prominent centers are in passage (Fig. 2a). The W-band EPR spectra of Center #6 are characterized by six main resonance absorption lines (Fig. 2a, b), indicative of six magnetically non-equivalent sites (Fig. 3a). The average linewidths of Center #6 are (∼0.1 mT at 77 K and ∼0.15 mT at 110 K, much narrower than their counterparts in the electron-irradiated quartz at corresponding temperatures. At a few orientations, Center #6 is characterized by the presence of a ^{29}Si hyperfine splitting between ∼0.40 and ∼0.46 mT (see also Mashkovtsev et al. 1978). However, this ^{29}Si hyperfine structure is usually obscured by other centers or too weak to be detected (i.e., natural isotope abundance of ^{29}Si = 4.7%) at most orientations. Therefore, it is not possible to quantitatively characterize the ^{29}Si hyperfine structure of Center #6.

The *g*-maximum value of Center #6 decreases slightly from 77 to 110 K, whereas its *g*-intermediate and *g*-minimum values show small increases (Table 1). The *g*-intermediate axis is ∼20° away from a twofold axis. The direction of the *g*-minimum axis is ∼11° away from the O2-O3 edge of the SiO_4 tetrahedron in the ideal quartz structure (Figs. 4, 5).

Center #7

Center #7, also not detectable at 298 K (Fig. 2c; Mashkovtsev et al. 1978), is visible at 77 and 110 K but is lower

Table 1 Spin-Hamiltonian parameters of six hole-like centers in natural citrine quartz at 77, 110 and 298 K

Center	Matrix **Y**				*K*k	Principal value	Principal direction		DP RMSD (mT)
						Y_k (°)	θ_k (°)	ϕ_k (°)	
#6 77 K	*g*	2.03290(1)	0.02090(1)	0.02468(1)	1	2.06807(2)	57.6(2)	36.7(2)	84
			2.02282(2)	0.01628(1)	2	2.00732(1)	69.5(2)	293.1(2)	0.095
				2.02153(1)	3	2.00187(1)	39.7(2)	176.5(2)	
#6	*g*	2.03269(2)	0.02062(2)	0.02455(1)	1	2.06762(2)	57.3(2)	36.6(2)	80
110 K			2.02261(2)	0.01612(1)	2	2.00740(2)	69.1(2)	292.5(2)	0.144
				2.02181(3)	3	2.00209(2)	40.2(2)	175.7(2)	
#7	*g*	2.03557(2)	−0.02642(2)	−0.00853(1)	1	2.05960(2)	76.0(2)	141.1(2)	102
77 K			2.02331(2)	0.00895(1)	2	2.00759(2)	22.1(2)	13.6(3)	0.164
				2.01011(2)	3	2.00179(2)	73.0(2)	235.4(2)	
B	*g*	2.00945(1)	−0.00308(1)	−0.00950(1)	1	2.03447(1)	21.3(2)	171.9(2)	372
110 K			2.00441(1)	0.00045(1)	2	2.00790(1)	71.6(2)	320.3(2)	0.156
				2.03077(2)	3	2.00226(1)	79.5(2)	53.8(2)	
	^{27}Al	−0.27(1)	−0.019(9)	−0.02(1)	1	−0.24(1)	62(11)	149(15)	
	A/$g_e\beta_e$ (mT)		−0.29(1)	0.01(1)	2	−0.30(1)	75(26)	246(19)	
				−0.30(1)	3	−0.31(1)	31(18)	1(51)	
B	*g*	2.00969(1)	−0.00298(1)	−0.01008(1)	1	2.03505(1)	22.1(2)	172.6(2)	576
298 K			2.00447(1)	0.00039(1)	2	2.00773(1)	71.1(2)	319.3(2)	0.161
				2.03095(1)	3	2.00234(1)	78.6(2)	53.2(2)	
	^{27}Al	−0.24(1)	−0.021(9)	−0.024(8)	1	−0.222(9)	65(7)	156(8)	
	A/$g_e\beta_e$ (mT)		−0.28(1)	0.013(7)	2	−0.292(8)	42(57)	36(65)	
				−0.282(9)	3	−0.300(8)	58(62)	263(43)	
B′	*g*	2.00964(2)	−0.00351(2)	−0.01006(1)	1	2.03555(2)	22.5(2)	165.5(2)	322
298 K			2.00461(2)	0.00178(1)	2	2.00771(2)	69.5(2)	319.5(2)	0.213
				2.03131(2)	3	2.00231(2)	80.9(2)	52.9(2)	
	^{27}Al	−0.30(2)	−0.02(1)	−0.03(1)	1	−0.27(2)	62(10)	156(9)	
	A/$g_e\beta_e$ (mT)		−0.34(2)	0.01(1)	2	−0.35(1)	107(9)	237(20)	
				−0.34(1)	3	−0.36(2)	33(9)	300(9)	
C′	*g*	2.00717(4)	−0.00215(1)	−0.00077(1)	1	2.01698(1)	30.7(2)	274.9(2)	163
298 K			2.00695(1)	−0.00582(1)	2	2.00823(3)	75.2(2)	158.6(2)	0.076
				2.01356(1)	3	2.00248(1)	63.7(2)	61.1(2)	
	^{27}Al	−0.18(4)	−0.03(1)	0.032(7)	1	−0.10(1)	53(7)	309(11)	
	A/$g_e\beta_e$ (mT)		−0.17(1)	−0.04(1)	2	−0.21(2)	57(57)	191(74)	
				−0.17(1)	3	−0.22(2)	52(55)	72(80)	
G′	*g*	2.01657(1)	0.00069(1)	0.01338(1)	1	2.02918(1)	46.7(2)	1.2(2)	295
110 K			2.00820(1)	−0.00027(1)	2	2.00828(1)	84.6(2)	266.1(2)	0.099
				2.01498(1)	3	2.00229(1)	43.7(2)	170.5(2)	
	^{27}Al	−0.49(1)	−0.043(7)	0.023(5)	1	−0.41(1)	54(4)	309(4)	
	A/$g_e\beta_e$ (mT)		−0.49(1)	−0.040(8)	2	−0.51(1)	39(9)	159(30)	
				−0.48(1)	3	−0.54(1)	74(16)	50(13)	
	^{27}Al	−0.01(7)	0.01(5)	0.01(9)	1	0.03(6)	52(93)	90(189)	
	P/$g_e\beta_e$ (mT)		0.01(7)	0.02(5)	2	0.00(8)	117(110)	157(163)	
				−0.002(80)	3	−0.03(6)	49(74)	220(131)	
G′	*g*	2.01670(1)	0.00063(1)	0.01336(1)	1	2.02925(1)	46.8(2)	0.7(2)	394
298 K			2.00800(1)	−0.00041(1)	2	2.00809(1)	84.2(2)	265.2(2)	0.125
				2.01502(1)	3	2.00238(1)	43.7(2)	169.2(2)	
	^{27}Al	−0.50(1)	−0.04(1)	0.024(7)	1	−0.41(1)	52(6)	307(4)	
	A/$g_e\beta_e$ (mT)		−0.48(1)	−0.040(8)	2	−0.51(1)	39(8)	146(30)	
				−0.476(9)	3	−0.54(1)	80(15)	44(13)	
	^{27}Al	−0.01(7)	0.01(4)	0.02(4)	1	0.03(3)	59(53)	53(78)	
	P/$g_e\beta_e$ (mT)		0.01(5)	0.01(5)	2	0.00(4)	120(100)	124(90)	
				−0.01(6)	3	−0.03(5)	45(86)	179(114)	

Spin-Hamiltonian parameters are given here for one of six symmetry-related sets. θ_k and φ_k (or equivalent 180 − θ_k and 180 + φ_k) are tilting angles relative to crystallographic c and a axes, respectively. *DP* number of line-position data points used in optimization. *RMSD* root-mean-sum of squares of the weighted difference between the calculated and observed line-position data

Table 2 Comparison of the principal g axes of the E_1' and hole-like centers in quartz

Center	Principal g values and directions							
	Literature data					This study (W-band)		
	g	θ (°)	φ (°)	Spectra	Ref.	g	θ (°)	φ (°)
E_1'	2.00179	114.5	227.7	X-band 300 K	1	2.00180(1)	114.4(1)	227.6(1)
	2.00053	134.5	344.4			2.00052(1)	134.7(6)	344.4(5)
	2.00030	125.4	118.7			2.00030(1)	125.2(6)	118.8(5)
#6	2.067(1)	57	270	X-band 77 K	2	2.06807(2)	57.6(2)	276.7(2)
	2.008(1)	90	0			2.00732(1)	69.5(2)	173.1(2)
	2.003(1)	33	90			2.00187(1)	39.7(2)	56.5(2)
#7	2.063	75	270	X-band 77 K	2	2.05960(2)	76.0(2)	278.9(2)
	2.007	90	0			2.00759(2)	22.1(2)	46.4(2)
	2.004	14	90			2.00179(2)	72.6(2)	184.6(2)
B	2.038(1)	158.2	18.5	Q-band RT	3	2.03505(1)	157.9(2)	−7.4(2)
	2.011(1)	107.9	162.1			2.00773(1)	108.9(2)	139.3(2)
	2.002(1)	77.9	76.0			2.00234(1)	78.6(2)	53.2(2)
B′						2.03555(2)	157.5(2)	−14.5(2)
						2.00771(2)	110.5(2)	139.5(2)
						2.00231(2)	80.9(2)	52.9(2)
C	2.01837(15)	26.7(10)	270	Q-band RT	4			
	2.0090(2)	90	0					
	2.0033(2)	63.3(10)	90					
C′						2.01698(1)	30.7(2)	274.9(2)
						2.00823(3)	75.2(2)	158.6(2)
						2.00248(1)	63.7(2)	61.1(2)
G	2.0325(4)	46.3(18)	0	Q-band RT	4	2.03102(1)[a]	46.6(1)	1.0(2)
	2.0109(5)	90	90			2.00809(1)	84.1(2)	265.4(2)
	2.0048(5)	43.7(18)	0			2.00235(1)	43.9(2)	169.3(2)
G′						2.02925(1)	46.8(2)	0.7(2)
						2.00809(1)	84.2(2)	265.2(2)
						2.00238(1)	43.7(2)	169.2(2)

Reference 1, Jani et al. (1983); 2, Mashkovtsev et al. (1978); 3, Maschmeyer et al. (1980); 4, Maschmeyer and Lehmann (1983)

[a] W-band data of Center G from Nilges et al. (2008). θ and φ are the tilting angles from the crystallographic c- and a-axis, respectively. Note that data for comparison with those in the literature are at corresponding temperatures. Also, symmetry-related sets of principal g axes are given for Centers #6 and #7 (in comparison with those in Table 1) to facilitate direct comparison with literature data

in intensity than Center #6 at similar magnetic field regions (Fig. 2a, b). The W-band spectra of Center #7 are characterized by six magnetically non-equivalent sites (Figs. 2a, b, 3b), with average linewidths of ~0.15 and ~0.5 mT at 77 and 110 K, respectively. The low intensity of this center, however, does not allow us to determine whether it possesses a ^{29}Si hyperfine structure or not (Mashkovtsev et al. 1978).

The g matrix of Center #7 at 77 K is given in Table 2. Quantitative analysis of this center at 110 K was not made owing to its considerable linewidth and low signal-to-noise ratios (Fig. 2b). The most notable feature of Center #7 is that the direction of its g-minimum axis is ~13° from the O1–O3 edge (Fig. 5).

Centers B and B′

The W-band EPR spectra measured at all three temperatures and microwave powers ≤2 mW show that "Center B" of Maschmeyer et al. (1980), as observed at X-band frequencies (Fig. 1), is a mixture of two similar centers (Fig. 2c). These two centers, which are both characterized by well-resolved ^{27}Al hyperfine structures with splittings between ~0.25 and ~0.36 mT, involve severe peak overlapping at most orientations, except for complete separations of ≤1 mT at low magnetic fields (Fig. 2c). Such small separations are impossible to resolve at X- and Q-band frequencies, particularly in the presence of unresolved ^{27}Al hyperfine structures. We designate the more

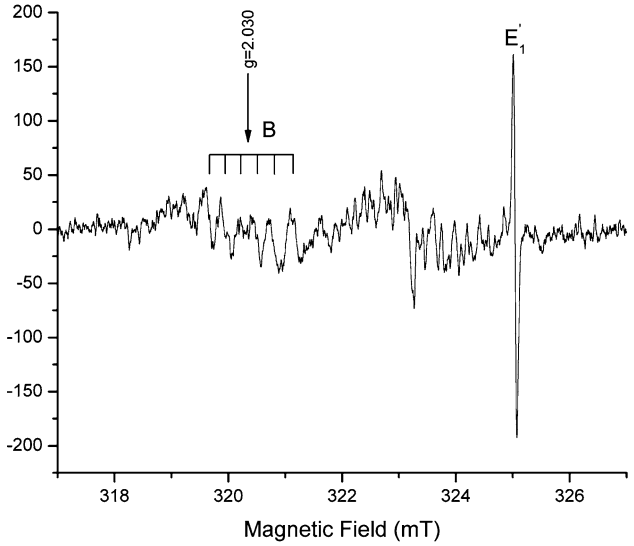

Fig. 1 Single-crystal X-band EPR spectrum of citrine quartz with magnetic field B approximately parallel to the crystallographic c axis, measured at a temperature of 298 K and a microwave power of 0.2 mW. Only Center E_1' and "Center B" at $g = 2.030$ are marked

prominent of these two centers as Center B and the other as Center B′ (Fig. 2c). Both Centers B and B′ are in passage at microwave powers ≥6.3 mW (Fig. 2a). The individual hyperfine lines of Centers B and B′ are similar in width of ∼0.1 mT, which does not appear to change significantly from 77 to 298 K.

Spin-Hamiltonian parameters of Center B at 110 and 298 K and Center B′ at 298 K are given in Table 1. The *g*-maximum and *g*-minimum values of Center B increase slightly from 110 to 298 K, while the *g*-intermediate value decreases (Table 1). The *g* matrices of Centers B and B′ are similar and are both characterized by *g*-intermediate and *g*-maximum axes ∼9° and ∼25° away from the O2–O4 and O2–O3 edges, respectively (Fig. 5). The ^{27}Al hyperfine structure of Center B is of approximately axial symmetry with the unique principal axis ($\mathbf{A_1}$) approximately along the bisector of the O2–Si2–O3 angle (Fig. 4). The ^{27}Al hyperfine structure of Center B′, which is slightly larger in size than that of Center B (Table 1), is also of approximately axial symmetry with the direction of the unique axis $\mathbf{A_1}$ again close to the bisector of the O2–Si2–O3 angle (Fig. 4).

Center C′

The W-band spectra measured at 298 K and 0.2 mW (Fig. 2c) disclose a center with principal *g* values similar to Center C of Maschmeyer and Lehmann (1983). This center, however, is distinct from Center C by its slightly larger ^{27}Al hyperfine structure (Table 1) and is hereafter referred to as C′. Center C′ is also visible in the 77 and 110 K spectra but is invariably low in signal-to-noise ratios. The individual hyperfine linewidths of Center C′ are (∼0.1 mT and do not change significantly from 77 to 298 K. Center C′, similar to Centers B and B′, is in passage at microwave powers ≥6.3 mW.

The direction of the *g*-maximum axis of Center C′ is only ∼5° away from the O3-O4 edge of the SiO_4 tetrahedron (Fig. 5). The A matrix of Center C′ is of approximately axial symmetry, with the direction of the unique axis ($\mathbf{A_1}$) approximately along the Si4–Si0 direction (Table 1, Fig. 4).

Center G′

The W-band spectra collected at all three temperatures and microwave powers between 0.2 and 2 mW disclose another new center with intensity second only to Center B (Fig. 2c). This center is hereafter referred to as Center G′, because it has a similar *g* matrix to the previously reported Center G (Table 2) but is distinct from the latter by its large ^{27}Al hyperfine structure (Maschmeyer and Lehmann 1983; Nilges et al. 2008). The well-resolved ^{27}Al hyperfine structure of Center G′ is characterized by splittings between 0.41 and 0.53 mT, which are considerably larger than those of other centers in Table 1 and are approaching those of the $[AlO_4]^0$ and $[AlO_4/M]^+$ centers (Walsby et al. 2003). However, the stability of Center G′ at 110 and 298 K distinguishes it from the $[AlO_4]^0$ and $[AlO_4/M]^+$ centers that are detectable only at ≤77 K (Walsby et al. 2003 and references therein). The average linewidth of Center G′ is (∼0.08 mT and does not change from 77 to 298 K. Similar to Centers B, B′ and C′, Center G′ is in passage at microwave powers ≥6.3 mW (Fig. 2a).

The *g*-maximum and *g*-minimum values of Center G′ increase slightly from 110 to 298 K, whereas its *g*-intermediate value decreases (Table 1). The directions of the *g*-maximum and *g*-minimum axes are (∼11° and ∼5° from the O1–O4 to O2–O3 edges, respectively (Fig. 5). The ^{27}Al hyperfine structure of Center G′ is also of approximately axial symmetry with the unique axis ($\mathbf{A_1}$) along the Si4–Si0 direction (Table 1; Fig. 4). The P matrices at 110 and 298 K, albeit with large uncertainties, are similar and are characterized by the direction of maximum anisotropy approximately along the Si4–Si0 direction (Table 1).

Discussion

The presence of the six hole-like centers in the natural citrine quartz without any artificial irradiation has also been confirmed by agreement between simulated and measured spectra at various orientations (Fig. 6). The similarity in X-band EPR spectra between the citrine quartz of this

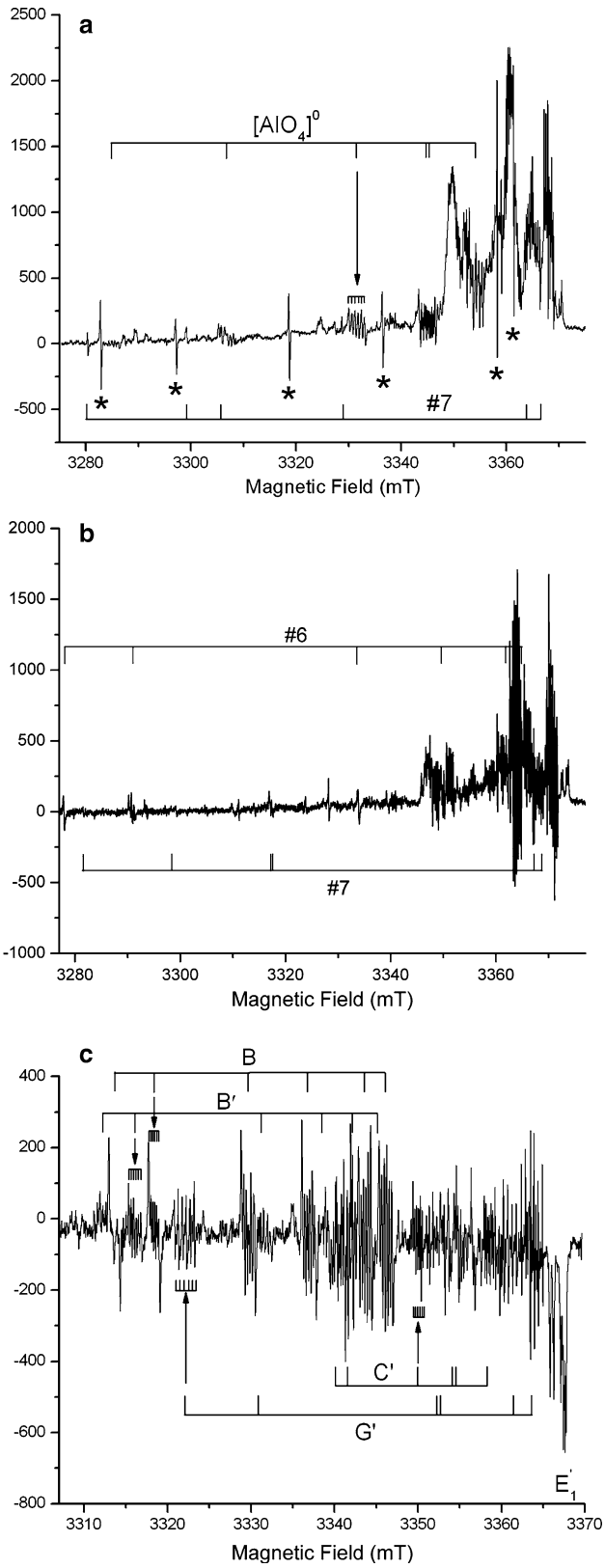

Fig. 2 Representative single-crystal W-band EPR spectra of citrine quartz: **a** spectrum measured at an orientation of $\theta = 90.1°$ and $\varphi = 238.3°$, 77 K and 6.3 mW to illustrate Centers #6 (*stars*), #7 and $[AlO_4]^0$, each consisting of six main resonance absorption peaks. Note that all other centers are in passage at this microwave power; **b** spectrum at $\theta = 113.0°$ and $\varphi = 195.5°$, 110 K and 2 mW, only Centers #6 and #7 are marked; and **c** spectrum at $\theta = 143.0°$ and $\varphi = 105.4°$, 298 K and 0.2 mW illustrating Centers B, B′, C′ and G′, all of which are characterized by well-resolved ^{27}Al hyperfine structures (marked at one site each only)

study and those from the uranium-rich Athabasca basin (Botis et al. 2008), together with the observation of Center #6 in an electron-irradiated sample (Nilges et al. 2008), supports these hole-like centers as natural radiation-induced defects (Mashkovtsev et al. 1978; Maschmeyer et al. 1980; Maschmeyer and Lehmann 1983).

Comparison with previous X- and Q-band EPR results

The single-crystal W-band spectra of natural citrine quartz confirm results of part I that Center #6 is characterized by six magnetically non-equivalent sites (Figs. 2a, b, 3a), contrary to a location on twofold axes suggested by the X-band EPR study of Mashkovtsev et al. (1978). Similarly, Center #7 is characterized by six magnetically non-equivalent sites (Figs. 2a, b, 3b) and hence does not reside on any special structural positions either. The fitted g matrices also show that none of the principal axes of Centers #6 and #7 coincides with any symmetry axes in quartz (Table 1). These results support our suggestion in part I that defect centers proposed to reside at special positions in the quartz structure by previous X- and Q-band EPR studies may be proven to deviate from symmetry elements at W-band or higher frequencies. Another notable difference between the results of Mashkovtsev et al. (1978) and this study is that the g-intermediate and g-minimum axes of Center #7 are switched (Table 2). We are more confident of results from the W-band EPR spectra, where all six magnetically non-equivalent sites are well resolved (Fig. 3b). The X-band spectra of Center #7 (Mashkovtsev et al. 1978), on the other hand, were difficult to analyze owing to severe line broadening related to unresolved site splittings.

The W-band spectra also show that "Center B" of Maschmeyer et al. (1980) is a mixture of two similar centers that are impossible to resolve at X- or Q-band frequencies. The g-maximum and g-intermediate values of both Centers B and B′ are significantly smaller than those reported by Maschmeyer et al. (1980) (Table 2). The g_{zz} value of ($\sim$2.030 for these centers in the X-band spectrum with **B//c** (Fig. 1) supports our results from W-band (Table 1) and shows that the values reported by Maschmeyer et al. (1980) are too large. Similarly, the g-maximum and g-intermediate values of Center G in Maschmeyer and Lehmann (1983) are notably larger than those reported by Nilges et al. (2008) (Table 2). The tilting angles of all three principal g axes from the c axis of Centers B and B′ are similar to those reported by Maschmeyer et al. (1980) (Table 2). The

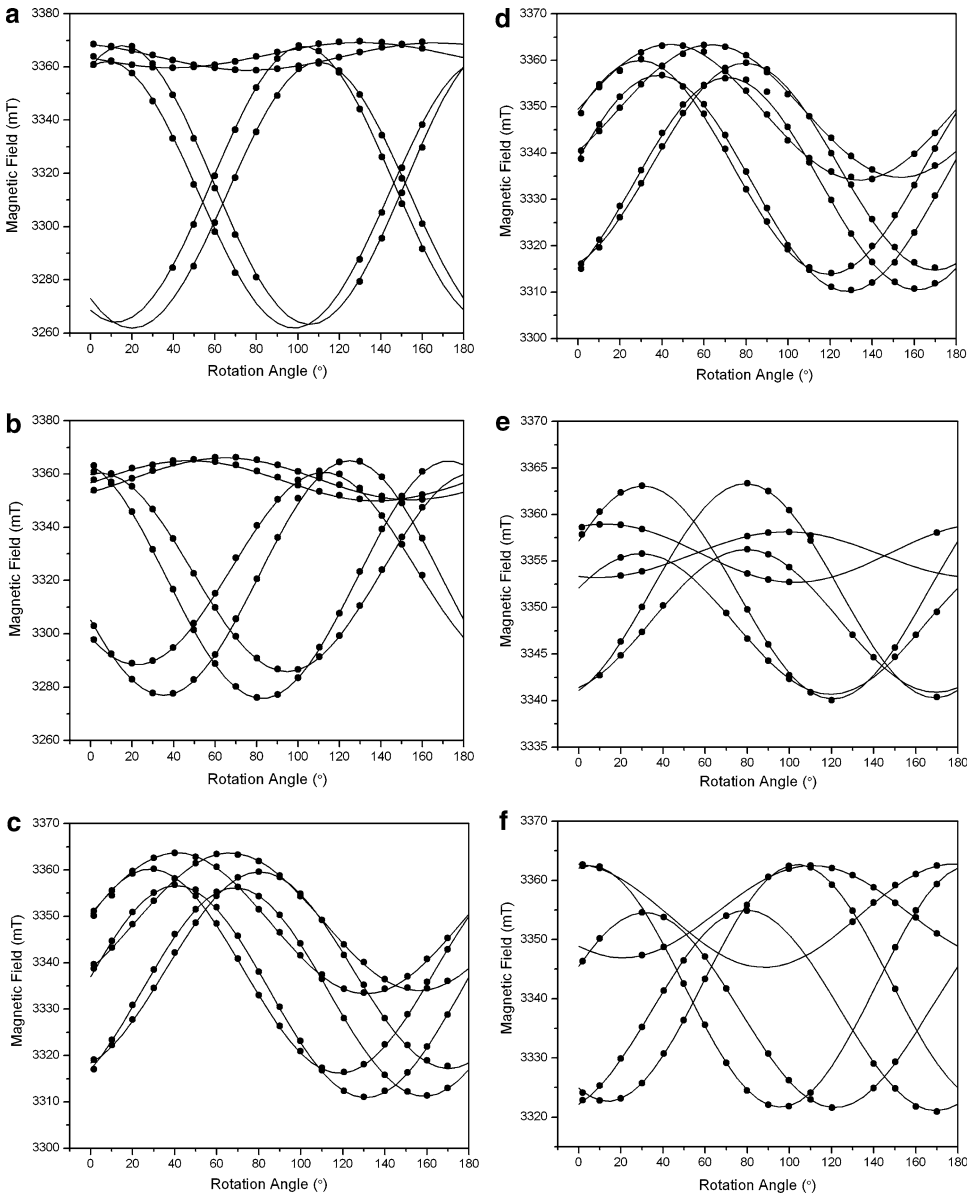

Fig. 3 Representative angular dependence ("line-position roadmap") of **a** Center #6 and **b** Center #7 at 77 K and **c** Center B, **d** Center B′, e) Center C′ and **f** Center G′ at 298 K in a plane with the normal of $\theta = 117.2°$ and $\varphi = 332.3°$, illustrating six magnetically non-equivalent sites each. *Solid circles* represent the observed data points; solid curves predicted by the spin-Hamiltonian parameters in Table 1. For clarity, only one ^{27}Al hyperfine line (m_I: +5/2 ↔ +5/2, which is an outer most transition) of each site is illustrated for Centers B, B′, C′ and G′

significantly different tilting angles of principal *g* axes from a twofold symmetry axis reported by Maschmeyer et al. (1980) are undoubtedly attributable to the superimposition of two similar centers in their X- and Q-band spectra.

By analogy with Centers #6 and #7, the directions of its principal *g* axes of Center C reported by Maschmeyer and Lehmann (1983) most likely include significant errors. It is possible that Centers C and C′, similar to Centers B and B′ and Centers G and G′, represent another pair of defects that have similar *g* matrices but different ^{27}Al hyperfine structures. Alternatively, Centers C and C′ are the same defect, and the A matrix reported by Maschmeyer and Lehmann (1983) was also in error.

This study exemplifies the value of W-band EPR studies for not only discrimination of defect centers with similar *g* matrices but also determination of their small local structural distortions that are often difficult to resolve in conventional X- and Q-band EPR studies. In addition, the advantage of single-crystal W-band EPR spectra in resolving ^{27}Al hyperfine structures of various sizes is noteworthy (Fig. 2c). For example, the ^{27}Al hyperfine structures of Centers B and B′, which were incompletely resolved in X- and Q-band spectra, are well resolved at W-band (Fig. 2c). One major factor is the minimization of peak overlapping either related to site splittings or involving centers of similar *g* values at W-band frequencies. Also, the nuclear Zeeman at W-band is much larger than the quadrupole coupling and the mixing of nuclear spin states is reduced, resulting in spectra insensitive to **P** and hence simpler ^{27}Al hyperfine patterns.

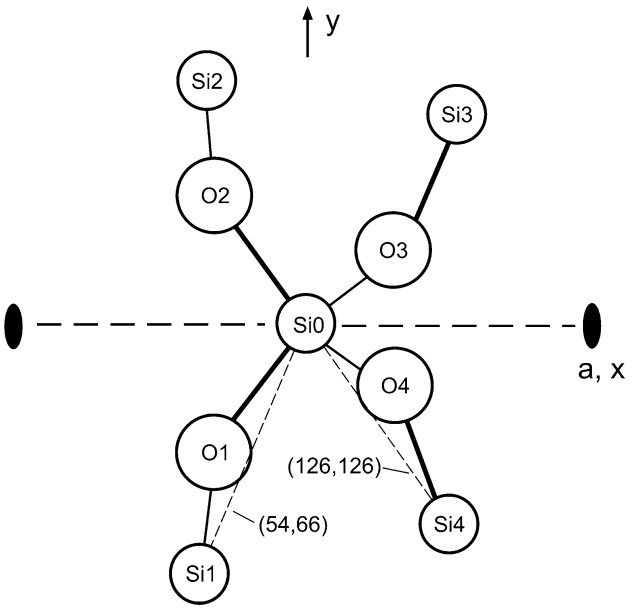

Fig. 4 A c-axis projection illustrating a SiO_4 tetrahedron and neighboring Si atoms in the right-handed α-quartz. Labels of the O and Si atoms are same as those in part I. The shorter Si–O bonds are marked by heavier lines. Also given are the Si1–Si0 and Si4–Si0 directions

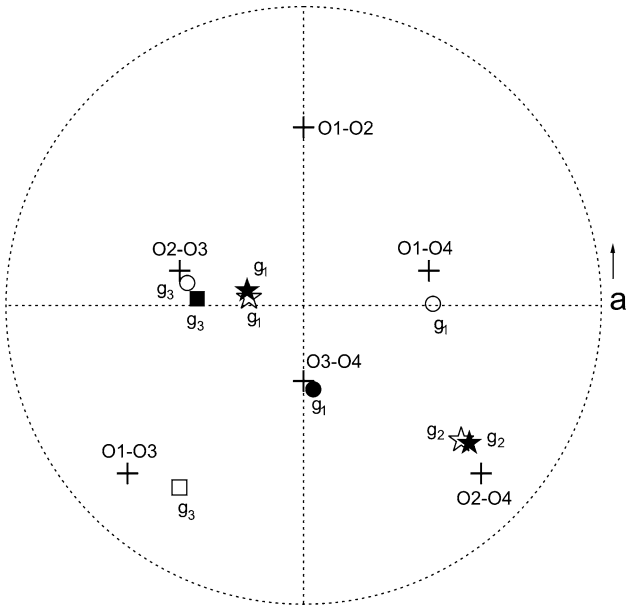

Fig. 5 Stereographic projection comparing the directions of selected principal *g* axes of six centers in citrine quartz with the O-O edges (crosses) of the SiO_4 tetrahedron in the ideal quartz structure. Note that the *g*-minimum principal axis (g_3) of Centers #6 (*solid square*) is ∼11° from the O2–O3 edge; g_3 of Center #7 (*open square*) are ∼13° from the O1–O3 edge; *g*-maximum axes (g_1) of Centers B (*solid stars*) and B′ (*open stars*) are ∼25° from the O2–O3 edge; and the *g*-intermediate (g_2) of Centers B and B′ are ∼9° from the O2–O4 edge; the *g*-maximum axis of Center C′ (*solid circle*) is ∼5° from the O3-O4 edge; and g_1 and g_3 of Center G′ (*open circles*) are ∼11° and ∼5° from O1–O4 and O2–O3 edges, respectively

Structural models

All six hole-like centers investigated in this study are characterized by one or two principal *g* axes approximately along the O–O edges of the SiO_4 tetrahedron in the quartz structure (Fig. 5). This type of geometry points to location of the unpaired spin on these O-O pairs. Possible structural models for defects of this type include O_2^{3-}, O_2^- and O_3^-, all of which have been proposed to arise from hole trapping on oxygen pairs associated with a missing central Si atom (Marfunin 1979; Botis et al. 2008). Difficulties and ambiguities in discriminating these structural models, particularly between O_2^{3-} and O_2^-, have been discussed in part I. The most useful feature for this purpose is the orientations of the principal *g* axes. For example, the O_2^{3-} type centers are characterized by *g*-minimum axes along O-O directions (Bill 1969), whereas both superoxide radicals (O_2^-) and ozonide radicals (O_3^-) have been shown to have *g*-maximum axes along O-O directions (Känzig and Cohen 1959; Schlick 1972). Also, the classic ozonide radicals in various hosts and on surfaces are known to have a similar average *g* value of (∼2.012 (Che and Tench 1983; Botis et al. 2008). Therefore, Centers #6 and #7 are most likely of the O_2^{3-} type, because their *g*-minimum axes are only ∼11° and ∼13° from the O2–O3 and O1–O3 edges, respectively (Fig. 5). These models are consistent with observed line-broadening of these centers from 77 to 110 K (and undetectable at 298 K), which is attributable to hole hopping between equivalent oxygen atoms and has been reported for other proposed O_2^{3-} centers (Bill 1969; Nilges et al. 2008). Peroxy radicals are known to be stable at 700 °C or higher (Friebele et al. 1979; Priest et al. 1991) and, therefore, are incompatible with Centers #6 and #7.

Nilges et al. (2008) suggested that Center G, on the basis of the geometry of the *g* matrix and the direction of the unique A axis, most likely represents a superoxide radical with the unpaired spin localized on the O1–O4 pair around a missing central Si atom and linked to a substitutional Al^{3+} ion at the neighboring Si4 site. Center G′ with a similar *g* matrix may also represent a superoxide radical with the unpaired spin localized on the same pair of oxygen atoms. The difference in the sizes of their ^{27}Al hyperfine structures can then be attributed to locations of the Al^{3+} ion at a different Si site. We note that Si1–Si0 and Si4–Si0 are symmetry-related in direction, but the Si1-O1 bond is longer than the Si4-O4 bond (Fig. 4). Therefore, substitutional Al^{3+} ions at the Si1 and Si4 sites, when interact with an unpaired electron on the O1–O4 pair, are expected to yield ^{27}Al hyperfine structures with similar directions of principal A axes but different sizes of splittings, as those observed for Centers G and G′. Therefore, Centers G and G′ are most likely superoxide radicals with the unpaired spin localized on the O1–O4 pair and linked to a

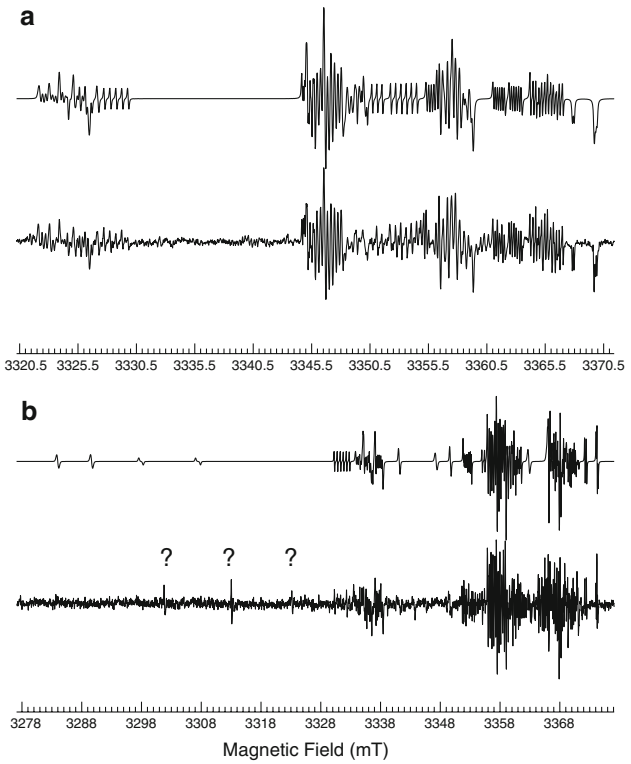

Fig. 6 Comparison of simulated and measured W-band spectra at selected orientations: **a** $\theta = 128.3°$ and $\varphi = 205.8°$ and 298 K, simulated spectrum (upper trace) includes Centers E_1', B, B′, C′ and G′; and **b** $\theta = 120.0°$ and $\varphi = 203.0°$ and 110 K, simulated spectrum includes Centers E_1', B, B′, C′ and G′, #6 and #7, also included are Centers D and E of Maschmeyer and Lehmann (1983), and unknown peaks are marked by ?

substitutional Al^{3+} ion at the neighboring Si1 and Si4 sites, respectively.

Similarly, Centers B and B′ have similar *g* matrices but different sizes of ^{27}Al hyperfine structures (Table 1). The directions of their principal *g* axes are compatible with either O_2^- or O_3^- models. However, the average *g* values of Centers B and B′ at 2.015 are significant larger than those of classic ozonide radicals at 2.012 (Che and Tench 1983; Botis et al. 2008 and references therein). Therefore, Centers B and B′ are probably superoxide radicals, with the unpaired spin on the O2–O3 pair and an Al^{3+} ion each at the Si2 and Si3 sites, respectively. These models are supported by the fact that the ^{27}Al hyperfine structures of Centers B and B′ are similar in the directions of principal A axes (Table 1) and that the A_1 axes (i.e., directions of maximum deviation from isotropic components) are close to the bisector of the O2–Si2–O3 angle. The size difference between the ^{27}Al hyperfine structures of Centers B and B′ is readily attributable to different Si2–O2 and Si3–O3 bond lengths. It is noteworthy that the *g*-maximum values of Centers B and B′ are similar to those of Centers G and G′ (Table 1) and are similar to those of other superoxide radicals linked to trivalent and quadrivalent cations in general (Lunsford 1973; Che and Tench 1983; Nilges et al. 2008). Also, the *g*-maximum value of another proposed superoxide radical in quartz (i.e., Centers #1 and F; Mashkovtsev et al. 1978; Maschmeyer and Lehmann 1983; Nilges et al. 2008) is similar as well.

The *g*-maximum axis of Center C′ along the O3–O4 edge is compatible with either a superoxide or ozonide model. The *g*-average value of Center C′ is similar to those of the classic ozonide radicals (Che and Tench 1983; Botis et al. 2008). Therefore, Center C′ probably represents an ozonide radical involving the O3–O4 edge around a missing central Si atom and linked to a subsitutional Al^{3+} ion at the neighboring Si sites. The A_1 axis of the ^{27}Al hyperfine structure along the Si4–Si0 direction suggests that the Al^{3+} ion is located at the neighboring Si4 site. Therefore, this center represents an Al-related variant of the ozonide radical reported by Botis et al. (2008), which involves the same O3–O4 edge but no Al^{3+} ion in the immediate-neighbor Si sites (see also Nilges et al. 2008).

Acknowledgments We thank the Natural Science and Engineering Research Council (NSERC) of Canada and the Denison Mines Corporation for financial support of this study, and Dr. M. Rieder, Dr. W.C. Tennant and an anonymous reviewer for incisive criticisms and helpful suggestions.

References

Azzoni CB, Meinardi F, Paleari A (1994) Trapped-hole centers in neutron-irradiated synthetic quartz. Phys Rev B49:9182–9185

Bill H (1969) Investigation on colour centres in alcaline earth fluorides. Helv Phys Acta 42:771–797

Botis SM, Nokhrin S, Pan Y, Xu Y, Bonli T, Sopuck V (2005) Natural radiation-induced damage in quartz. I. Correlations between cathodoluminescence colors and paramagnetic defects. Can Mineral 43:1565–1680

Botis SM, Pan Y, Nokhrin S, Nilges MJ (2008) Natural radiation-induced damage in quartz. III. A new ozonide radical in drusy quartz from the Athabasca basin, Saskatchewan. Can Mineral 46:121–135

Che M, Tench AJ (1983) Characterization and reactivity of molecular oxygen species on oxide surfaces. Adv Catal 32:1–148

Friebele EJ, Griscom DL, Stapelbroek M, Weeks RA (1979) Fundamental defect centers in glass: the peroxy radical in irradiated, high-purity, fused silica. Phys Rev Lett 42:1346–1349

Garrison EG, Rowlett RM, Cowan DL, Holroyd LV (1981) ESR dating of ancient flints. Nature 290:44–45

Griscom DL, Friebele EJ (1981) Fundamental defect centers in glass: ^{29}Si hyperfine structure of the non-bridging oxygen hole center and the peroxy radical in SiO_2. Phys Rev B 24:4896–4898

Ikeya M (1993) New applications of electron paramagnetic resonance: ESR dating, dosimetry, and spectroscopy. World Scientific, Singapore, p 500

Jani MG, Bossoli RB, Halliburton LE (1983) Further characterization of the E_1' centre in crystalline SiO_2. Phys Rev B 27:2285–2293

Känzig W, Cohen MH (1959) Paramagnetic resonance of oxygen in halides. Phys Rev Lett 3:509–510

Lunsford JH (1973) ESR of adsorbed oxygen species. Cat Rev 8:135–156

Mackey JH, Boss JW, Wood DE (1970) EPR study of substitutional-aluminum-related hole centers in synthetic α-quartz. J Magn Reson 3:44–54

Marfunin AS (1979) Spectroscopy, luminescence and radiation centers in minerals. Springer, Berlin, p 352

Maschmeyer D, Niemann K, Hake H, Lehmann, Räuber A (1980) Two modified smoky quartz centers in natural citrine. Phys Chem Miner 6:145–156

Maschmeyer D, Lehmann G (1983) New hole centers in natural quartz. Phys Chem Miner 10:84–88

Mashkovtsev RI, Shcherbakova MYa, solntsev VP (1978) EPR of radiation oxygen hole centers in α-quartz. Tr Inst Geol Geofiz, Akad Nauk SSSR, Sib Otd 385:78–86 (in Russian)

Mombourquette MJ, Weil JA, McGavin DG (1996) EPR-NMR users' manual. Department of Chemistry, University of Saskatchewan, Saskatoon

Nilges MJ, Smirnov AI, Clarkson RB, Belford RL (1999) Electron paramagnetic resonance W-band spectrometer with a low-noise amplifier. Appl Magn Reson 16:167–183

Nilges MJ, Pan Y, Mashkovtsev R (2008) Radiation-induced defects in quartz. Part I. Single-crystal W-band EPR study of an electron-irradiated quartz. Phys Chem Miner 35:103–115

Priest V, Cowan DL, Yasar H, Ross FK (1991) ESR, optical absorption, and luminescence studies of the peroxy-radical defect in topaz. Phys Rev B44:9877–9882

Rossman GR (1994) Colored varieties of the silica minerals. Rev Miner 29:433–467

Samoilovich MI, Tsinober LI, Kreiskop VN (1969) The nature of radiation-produced citrine coloration in quartz. Sov Phys Crystallogr 13:626–628

Samoilovich MI, Tsinober LI, Dunin-Barkovsky RL, Lisitsina EE, Khadzhy VE (1976) About the third type of citrine color of natural quartz. Zap Vses Min Obsh 105:223–227 (in Russian)

Schlick S (1972) ESR spectrum of O_3^- trapped in a single crystal of potassium chlorate. J Chem Physc 56:654–661

Schmetzer K (1989) Methods for the distinction of natural and synthetic citrine and prasiolite. J Gemmology 21:368–391

Walsby CJ, Lees NS, Claridge RFC, Weil JA (2003) The magnetic properties of oxygen-hole aluminum centres in crystalline SiO_2. VI: a stable AlO_4/Li centre. Can J Phys 81:583–598

Weil JA (1984) A review of electron spin resonance and its applications to the study of paramagnetic defects in crystalline quartz. Phys Chem Miner 10:149–165